ORIGINAL PAPER

Development of a pressure-driven nanofluidic control system and its application to an enzymatic reaction

**Takehiko Tsukahara · Kazuma Mawatari ·
Akihide Hibara · Takehiko Kitamori**

Abstract A novel air-pressure-based nanofluidic control system was developed and its performance was examined. We found that the flow in a 100 nm scale nanochannel on a chip (called an extended nanospace channel) could be controlled within the pressure range of 0.003–0.4 MPa, flow rate range of 0.16–21.2 pL/min, and residence time range of 24 ms–32.4 s by using the developed nanofluidic control system. Furthermore, we successfully demonstrated an enzyme reaction in which the fluorogenic substrate TokyoGreen-β-galactoside (TG-β-gal) was hydrolyzed to the fluorescein derivative TokyoGreen (TG) and β-galactose by the action of β-galactosidase enzyme as a calalyst in a Y-shaped extended nanospace channel. The parameters for the reaction kinetics, such as K_m, V_{max} and k_{cat}, were estimated for the nanofluidic reaction, and these values were compared with the results of bulk and microfluidic reactions. A comparison showed that the enzyme reaction rate in the Y-shaped extended nanospace channel increased by a factor of about two compared with the rates in the bulk and micro spaces. We thought that this nanospatial property resulted from the activated protons of water molecules in the extended nanospace. This assumption was supported by the result that the pH dependence of the maximum enzyme activity in the Y-shaped extended nanospace channel was slightly different from that in the bulk and micro spaces.

T. Tsukahara · A. Hibara · T. Kitamori (✉)
Department of Applied Chemistry, School of Engineering,
The University of Tokyo,
7-3-1 Hongo,
Bunkyo-ku, Tokyo 113-8656, Japan
e-mail: kitamori@icl.t.u-tokyo.ac.jp

T. Tsukahara · K. Mawatari · T. Kitamori
Core Research for Evolutional Science and Technology (CREST),
Japan Science and Technology Agency,
4-1-8 Honcho,
Kawaguchi, Saitama 332-0012, Japan

K. Mawatari · A. Hibara · T. Kitamori
Kanagawa Academy of Science and Technology (KAST),
Sakado, Takatsu-ku,
Kawasaki, Kanagawa 213-0021, Japan

Introduction

One-nanometer-scale materials such as a carbon nanotubes, zeolite, and self-assembled polymers can show quantum-sized and optical near-field effects. Various nanophotonics and nanoelectronics devices have been realized by skillfully utilizing nanospatial characteristics [1–3]. When water molecules are confined in such nanospaces, the behavior of these water molecules is quite different from that of water molecules in the bulk. A variety of experimental and theoretical studies have shown that confined water has more ordered hydrogen-bonding structures and slower molecular motions than bulk water, and that the specific properties play an important role in determining the functions of cell signaling, protein refolding, chromatography separation, and so on [3–9].

On the other hand, at the micrometer scale, which is three orders of magnitude larger than one-nanometer-scale material, studies on microchemical systems have been advancing rapidly. The fluidics in micrometer-scale spaces are dominated by laminar flow, molecular diffusion, and liquid–liquid and liquid–solid interface areas per unit

volume, while the physicochemical properties of liquids in microspaces are not influenced by space sizes. By using the characteristics of microfluidics in a microchemical chip, effective molecular transport, chemical and enzymatic reaction controls, and biochemical analyses have been demonstrated [10–15]. We have also developed a concept for continuous flow chemical processing (CFCP), which is based on a combination of micro unit operations (MUOs) and a multiphase flow network using pressure-driven microflows, and we have miniaturized complicated micro chemical systems for analysis, synthesis, diagnosis, and immunoassay on a microchip [16]. Moreover, synthetic and enzymatic reactions are accelerated in micrometer-scale spaces, unlike bulk reactions [17, 18].

The 10–100 nm scale space (called the extended nanospace), which is a technologically unexplored region between one-nanometer-scale material and microchemical chips, is expected to be a promising experimental area for implementing highly integrated micro/nanofluidic devices and understanding molecular physical chemistry. Actually, we have developed two-dimensional (2-D) extended nanospaces using top-down-type micro/nanofabrication technologies, and we have achieved liquid introduction and mixing in them [19, 20]. Several researchers have also demonstrated the electrophoretic transport of ionic species and the manipulation of single molecules by electroosmotic flow in fabricated one-dimensional (1-D) extended nanospaces [21–26]. From the viewpoint of molecular physical chemistry, since the extended nanospace is a area of transition in molecular behavior from that of individual molecules to that of the bulk condensed phase, this space can be applied to characterize the collective properties of liquid-phase molecular clusters of 10–100 nm size. A 1-nm-scale space like that found in nanomaterials is too small to handle liquid-phase molecules. To this end, we carried out capillarity and time-resolved fluorescent measurements of water confined in a 2-D extended nanospace and found that the water confined in the 330 nm-sized extended nanospace has a higher viscosity and a lower dielectric constant than bulk water [27]. Furthermore, in order to clarify the size-confinement mechanisms, we have examined molecular structures and dynamic properties of water confined in various extended nanospaces using NMR spectroscopy [28]. The results showed that water shows slower translational motion and higher proton mobility with decreasing space size, while hydrogen-bonding structures and molecular rotations do not depend on the space size. Such properties appeared in channel sizes below 800 nm. Based on these results, we inferred that an intermediate phase consisting of loosely coupled water molecules located within ~50 nm of the surface existed in extended nanospaces.

It is expected that these unique properties of water in extended nanospaces affect chemical reactions, and that a

nano chemical reaction is quite different from that in a microspace. Thus, it is essential to control the nanofluidics precisely in extended nanospaces and to evaluate chemical reaction mechanisms and molecular transport phenomena in them. Taking this viewpoint, we previously developed a backpressure-based nanofluidic control system and demonstrated a fluorescence reaction of fluorescein dye molecules in a Y-shaped 100-nm-scale nanochannel on a chip (called an Y-shaped extended nanospace channel) [29]. However, since this system depended on the response times of the backpressure regulators, chaotic flow conditions such as backward flow or plug-like flow took place in the nanospace channel. In order to control the reaction and residence times in the Y-shaped extended nanospace channel, both a high pressure (of MPa) and a low volume flow rate (of pL/min) is required to develop nanofluidic control systems because of the relatively large pressure drop in extended nanospaces. Hence, in the present study, we construct an air-pressure-based nanofluidic control system and evaluate its performance. Then we perform an enzymatic reaction, one of the most important chemical reactions, in a Y-shaped extended nanospace channel using the novel air-pressure-driven nanofluidic control system. Based on these results, we discuss size-confinement effects for the kinetic parameters of enzymatic reactions.

Experimental

Materials

Electron beam resist (ZEP-520A, Zeon Corp., Tokyo, Japan), conductive polymer (Espacer300, Showa Denko K.K., Tokyo, Japan), o-xylene, dimethyl sulfoxide (DMSO), 2-propanol, sulfuric acid, and hydrogen peroxide (Kanto Chemical, Tokyo, Japan) were utilized for micro/nanofabrications. Negative photoresist SU-8 was obtained from MicroChem (Newton, MA, USA). Pure Cr metal film (Nilaco, Tokyo, Japan) were used in the sputtering process. The β-galactosidase (β-gal, *Escherichia coli*, 500 unit/mg) and fluorogenic substrate, TokyoGreen-β-galactoside (TG-β-gal), were purchased from Funakoshi Corp. and Daiichi Pure Chemicals Co. Ltd. (Tokyo, Japan), respectively. The TG-β-gal has been designed as a fluorescence probe molecule for β-galactosidase. 4-(2-Hydroxyethyl)-1-piperazineethanesulfonic acid (HEPES), 2-mercaptoethanol, and $MgCl_2$ were obtained from Wako Pure Chemical Industries, Ltd. (Osaka, Japan). A stock solution of β-gal was prepared in a 10-mL total volume of 100 mM HEPES buffer containing 20 mM 2-mercaptoethanol, 1 mM $MgCl_2$, and 0.1% DMSO for the pH range of 7.0–9.0. TG-β-gal was obtained as a 250-μM stock solution, and this was diluted with HEPES buffer (pH 7.0–9.0) to the desired

concentration. All ultrapure water samples were treated with a water purification system comprising a reverse osmosis membrane, ion exchange cylinder, and UV sterilizer (Minipure TW-300RU, Nomura Micro Science Co., Ltd., Kanagawa, Japan), yielding a specific resistivity greater than 18.0 MΩ cm.

Micro and nanofabrications

As the fabrication procedures in this study were essentially the same as those described in our previous papers [27–29], except for a few changes, only an outline is given here. A 0.7-mm-thick synthetic quartz glass substrate (VIOSIL-SX, ShinEtsu Quartz Co., Ltd., Tokyo, Japan) with 30× 70 mm sides was coated with electron beam resist and conductive polymer using a spin coater. Electron beam lithography (ELS-7500, Elionix Co., Ltd., Tokyo, Japan) was used to draw a Y-shaped extended nanoscale pattern onto the substrate. The nanopattern drawn was developed in o-xylene, rinsed in 2-propanol, and fabricated by plasma etching (NE-550, ULVAC Co., Ltd., Kanagawa, Japan) using a mixture of CF_6 and CHF_3 gases. The fabricated extended nanospace channel consisted of an introduction part (nanochannel A = width, 400 nm; depth, 234 nm; length, 500 μm) and a mixing part (nanochannel B = width, 620 nm; depth, 234 nm; length, 200 μm). The sizes were determined from images obtained with a scanning electron microscope (SEM) and an atomic force microscope (AFM; SPA-400, SII NanoTechnology Inc., Chiba, Japan). After a thin Cr layer (~50 nm) was sputtered onto the substrate, U-shaped microchannels (200 μm wide and 8 μm deep) were fabricated by photolithography and plasma etching. These U-shaped microchannels were used to introduce solutions and were located on both sides of the extended nanospace channel. Inlet holes were pierced through the patterned substrate using a diamond-coated drill. The substrate was then washed repeatedly in o-xylene, DMSO, ultrapure water, and a mixed solution of sulfuric acid and hydrogen peroxide (3:1), before being thermally laminated with a cover plate in a vacuum furnace at 1080 °C (KDF-900GL, Denken Co., Ltd., Oita, Japan). All operations were carried out in the clean rooms (classes 100, 1,000, and 10,000) to exclude impurities.

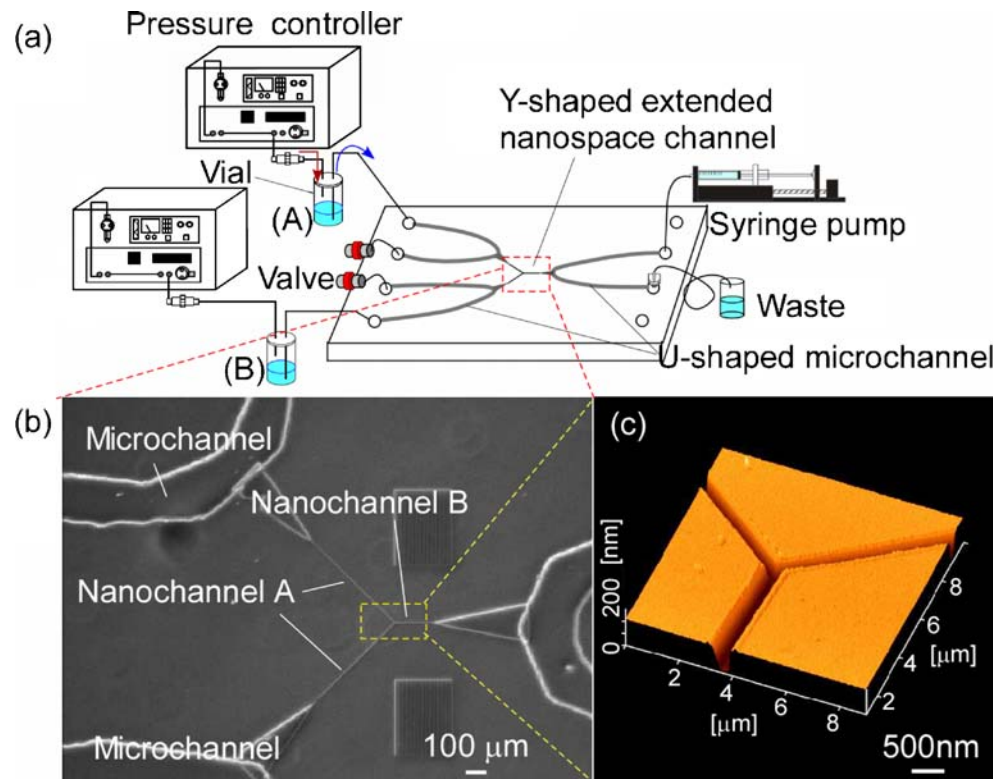## Bulk and microfluidic control systems

To compare the results of the extended nanoscale reaction with those of the bulk and microscale reactions, we carried out bulk and microfluidic enzyme reactions. The bulk reaction was examined using a standard quartz cuvette (10 mm in depth and width and 40 mm in height) as a reaction vessel. The reaction was initiated by adding fluorogenic substrate solution to enzyme solution. The temperature was controlled by a temperature controller at 32 °C. On the other hand, for a microscale reaction, a glass microchip equipped with a Y-shaped microchannel (100 μm wide, 40 μm deep, and 40 mm long) was used. The fabrication procedures have been described elsewhere [17]. In brief, the Y-shaped microchannel was etched onto a rectangular Pyrex glass substrate with 30 mm×70 mm sides and 0.7 mm thickness by a conventional photolithographic wet-etching technique. A diamond-coated drill was used to bore inlet and outlet holes into the etched substrate. After the etched substrate and a cover plate were chemically washed, they were laminated by a thermal bonding method at 650 °C for 24 h. The enzyme and substrate solutions were introduced through the two inlets onto the microchip using a micro-syringe pump (model 200 series; KD Scientific, Holliston, MA, USA). The solutions could be diffusion-mixed after the Y-intersection. After the flow was stopped, the time dependence of the reactions was examined in the microchannel. The temperature of the microchannel was controlled to an accuracy of 32±0.5 °C using a Peltier stage, which iconsists of an ITO (indium tin oxide) electrode coated onto a glass and a chip holder (see the "Electronic Supplementary Material").

Setup of air-pressure-based nanofluidic control system

The pressure balance before the Y-intersection is one of the most important factors to consider when attempting to realize stable flow in a Y-shaped extended nanospace channel. Buffer air is expected to be suitable as a pressure source for stable pressurizing. Figure 1 shows a schematic illustration of the air-pressure-based nanofluidic control system, including an Y-shaped extended nanospace channel. The sample solution (A) was poured into a vial, which had two gateways. The outlet was connected through a capillary tube to one of the U-shaped microchannels on the chip, and the inlet was connected through 1/16 inch stainless steel tubing to one of the air-pressure controllers. Air was pressurized into a sample solution (A) from the inlet by using the air-pressure controller, and the sample solution (A) in the vial was delivered to one side of the U-shaped microchannel from the outlet of the vial. After the valve that was connected to the other side of this U-shaped microchannel was closed, the sample solution (A) inside the microchannel could be introduced into the Y-shaped extended nanospace channel based on the pressure-driven flow. In this system, the pressures in the U-shaped microchannel and Y-shaped extended nanospace channel were kept constant. When the sample solution (B) was similarly introduced, the two different solutions (A) and (B) could be diffusion-mixed in the Y-shaped extended nanospace channel. The molecular diffusion distance in the nanochannel is quite short, and solution mixing can be achieved

in milliseconds. The pressure was controlled by the air-
pressure controllers to an accuracy of ± 0.001 MPa, and its
value in the nanochannel was confirmed with a pressure
gauge connected the outlet part of the microchannel.

## Results and discussion

Performance of the air-pressure-based nanofluidic control system

In order to evaluate the performance of the nanofluidic
control system, we examined the variation in fluorescence
intensities generated by mixing two different solutions: an
aqueous solution of the fluorescein derivative TG ($5.0 \times
10^{-5}$ M) and HEPES buffer solution (pH 8.0). A fluores-
cence image of the TG solution at 0.1 MPa is shown in
Fig. 2. We found that the TG solution flowed from nano-
channel A to nanochannel B without backward flow into the
other side of nanochannel A or plug-like flow. When the
fluorescence intensities of the TG solutions in nanochannels
A and B were compared with each other, nanochannel B was
found to have about an intensity that was 0.6 times lower than
that in nanochannel A. When the introduction of TG solution
and HEPES buffer solution into nanochannel A was switched
each other, i.e., a fluorescence image of TG as shown in Fig. 2
was upside down, this fluorescence intensity ratio was did
not change. The phenomenon in which the intensity ratio of
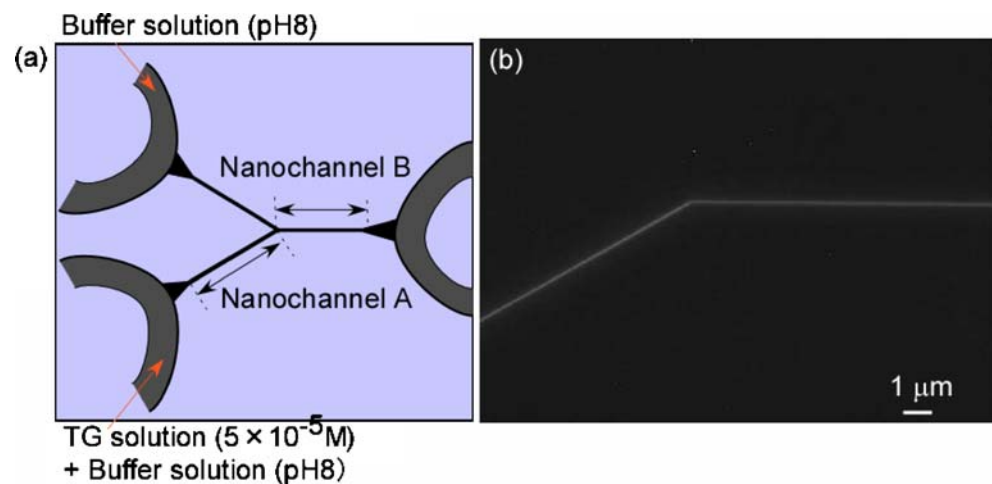
nanochannel A to nanochannel B was not 1.0:0.5 but 1.0:0.6 could be caused by differences in position resolution in the observed fluorescence images. Furthermore, we measured the fluorescence intensities of TG solutions with various known pH values. A plot of relative fluorescence intensity vs. pH for the TG solutions showed that the intensity ratio of 1.0:0.6 was almost the same over the whole pH range (Fig. 3a). These results indicated that mixing equal quantities of TG solutions could be realized in the Y-shaped extended nanospace channel.
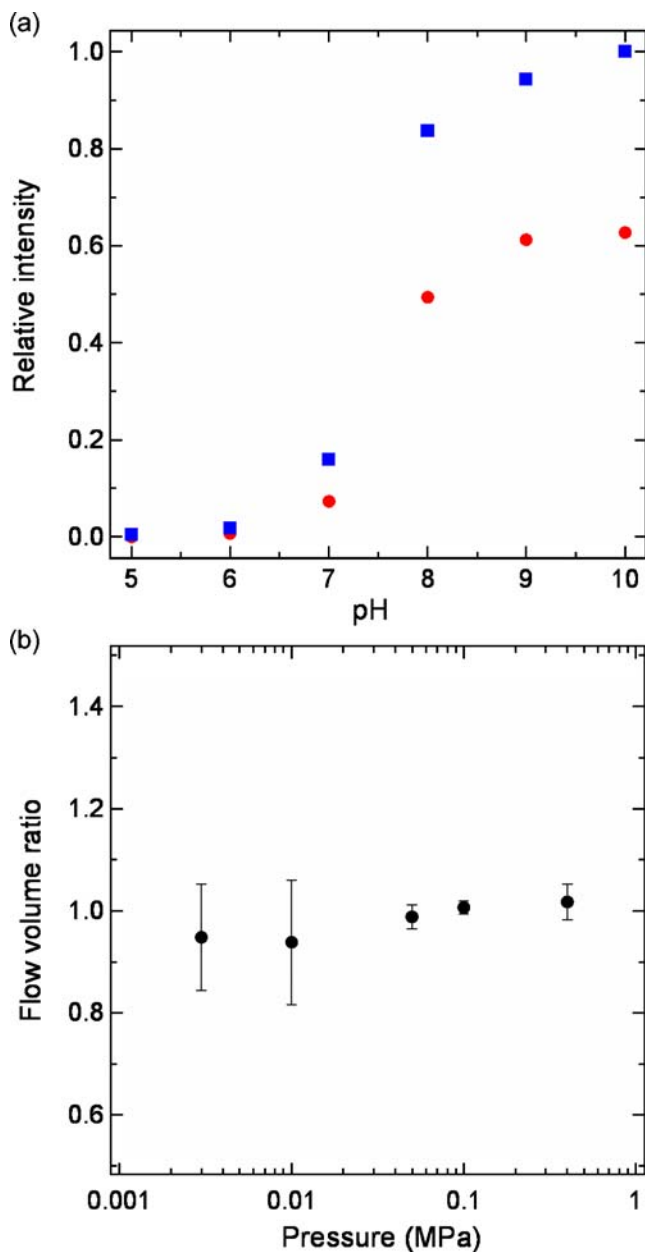
Fig. 3 a Plot of relative fluorescence intensity vs. pH for TG solutions in nanochannel A (*squares*) and nanochannel B (*circles*). The fluorescence intensities are normalized to that of the TG solution in nanochannel A at pH10. b Plot of flow volume vs. pressure of the TG solution in the Y-shaped extended nanospace channel

Furthermore, the fluorescence intensities of the TG solutions were measured for pressures of 0.001–0.5 MPa. The TG solutions flowed stably in the nanochannel without the appearance of backward and plug flows in the pressure range of 0.003–0.4 MPa, as shown in Fig. 3b. Since the pressure obtained is related to the pressure drop (ΔP) in the nanochannel, the ΔP value is theoretically expressed by Hagen–Poiseuille's law as follows:

$$\Delta P = \frac{128 \mu V l}{\pi d^4} \qquad (1)$$

where d is the equivalent diameter of the channel , l is the channel length, V is the flow rate, and μ is the viscosity. As the ΔP value was increased from 0.003 to 0.4 MPa at a μ value of 1 cP, the V value increased from 0.16 to 21.2 pL/min in nanochannel B. In this case, the flow velocities in nanochannel A were found to be almost the same as those in nanochannel B over the whole pressure range. The residence times of the solutions in nanochannel B were related to the V values, and could be estimated as ~8 ms–10.8 s. It is worth noting that our previous studies showed that the speed of introduction of the water into the 300 nm-sized nanochannels was slower than that predicted by Hagen-Poiseuille's law in a microchannel, and that the mass flow rate of the aqueous solution containing the probe molecules in a 300 nm-sized nanochannel was also lower than that estimated from the law [27, 29]. These results mean that the actual liquid flow rate in the nanochannel was about three times slower than that of bulk liquid. Accordingly, when the solutions in nanochannel B were transferred from the mixing point to the outlet point at ΔP=0.003 MPa, about 32 s were required. This nanofluidic system provides enough time to measure the progress of enzymatic reactions in the extended nanospace.

Bulk and microfluidic enzyme reactions

In order to evaluate the size-confinement effects for an enzyme reaction, bulk, microfluidic, and nanofluidic enzyme reactions were carried out at pH of 7.5. As a suitable enzymatic reaction for these spaces, we selected a hydrolysis reaction in which nonfluorescent TG-β-gal was hydrolyzed to TG and β-galactose by β-gal acting as catalyst, as shown in Fig. 4a. The excitation wavelength was 490 nm, and the observed reaction product, which was TG, exhibited strong fluorescence at around 510 nm. The bulk reaction was monitored with a fluorescence spectrophotometer (F-4500, Hitachi, Ltd., Tokyo, Japan) at 511 nm. To begin with, the bulk reaction was initiated by adding 0.5 mL of β-gal to 0.5 mL TG-β-gal solution (100 μM) in a cuvette for a final enzyme concentration of 5 μM. The time course of the fluorescence intensity of the reaction product TG was measured for a period of 30 s, and the fluorescence intensities were found to increase continuously with time.
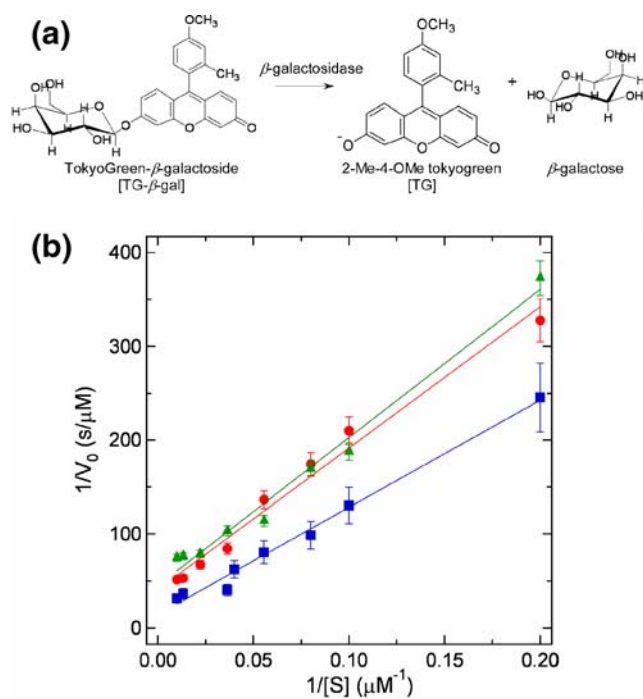
Fig. 4 **a** Reaction scheme for the β-gal catalyzed hydrolysis of TG-β-gal. **b** Lineweaver–Burk plot of the initial rate V_0 vs. TG-β-gal substrate concentration for bulk (*triangles*), microfluidic (*circles*), and nanofluidic (*squares*) reactions at pH 7.5

Moreover, the slope of the plot of the fluorescence intensity vs. time was examined in the TG-β-gal concentration range of 5–100 μM. We found that the slope increased with increasing TG-β-gal concentration.

In general, the slope corresponds to the initial reaction rate of the enzyme reaction, V_0, and the V_0 values can be expressed by the Michaelis–Menten equation:

$$\frac{1}{V_0} = \frac{K_m}{V_{max}} \frac{1}{[S]} + \frac{1}{V_{max}} \qquad (2)$$

where K_m is the Michaelis constant, V_{max} is the maximum reaction rate, and $[S]$ is the substrate concentration. Therefore, a Lineweaver–Burk plot of $1/V_0$ vs. $1/[S]$ was used to determine the kinetic parameters of the bulk reaction. These results are shown in Fig. 4b. The unit of V_0 was converted from fluorescence intensity to concentration. We found that the $1/V_0$ values decreased continuously with decreasing concentration. The K_m and V_{max} values were obtained from the slope of the line and the intercept in Fig. 4b, as listed in Table 1. Moreover, the first-order rate constant of the enzyme reaction, k_{cat}, was related to the total enzyme concentration $[E]_t$ as follows:

$$k_{cat} = \frac{V_{max}}{[E]_t} \qquad (3)$$

According to Eq. 3, k_{cat} was 4.4×10^{-3} s^{-1}.

To determine the kinetic parameters for the microfluidic enzyme reaction, the TG-β-gal and β-gal solutions were

introduced into a Y-shaped microchannel through the two inlets at flow rates of 10 μL/min. After the flow in this microchannel was stopped, the fluorescence of TG (produced by the enzyme reaction) was monitored in the microchannel on the microchip using a fluorescence microscope (IX70, Olympus, Tokyo, Japan), an objective lens (Olympus, ×4, NA 0.13 or Olympus, ×10, NA 0.25), and a cooled CCD camera (Pentamax Gen IV, Roper Scientific GmbH, Ottobrunn, Germany). The fluorescence was scanned across the microchannel and then the average of the measured fluorescence intensities was obtained, as shown in Fig. S1 (see the Electronic Supplementary Material). The difference between the average fluorescence intensity and the background intensity was adopted as the fluorescence intensity at a particular time. The time dependence of the fluorescence intensity was measured in the TG-β-gal concentration range of 5–100 μM for a period of 30 s. The results showed that the fluorescence intensity increased over time and as the TG-β-gal concentration increased. Therefore, the reciprocal of the slope, $1/V_0$, was plotted against the reciprocal of the TG-β-gal concentration, $1/[S]$ (Fig. 4b), together with the results for the bulk reaction. The K_m, V_{max}, and k_{cat} values for the microfluidic reaction were found to be similar to those for the bulk reaction (Table 1).
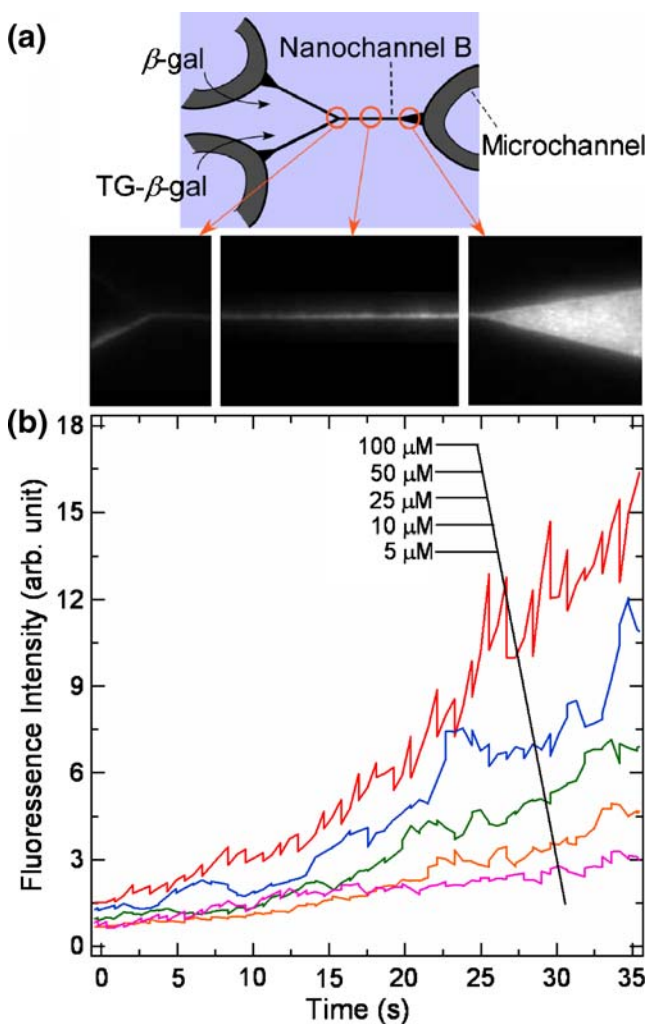
Nanofluidic enzyme reaction

Next, we used our air-pressure-based nanofluidic control system to examine an enzyme reaction in the Y-shaped extended nanospace channel. The same concentration range was used for the nanofluidic as for bulk and microfluidic reactions. The TG-β-gal and β-gal solutions were introduced into the Y-shaped extended nanospace channel through the two inlets, and the reaction was initiated after the Y-intersection. Since the pressure established by the pressure controllers was 0.003 MPa, the reaction time in the nanochannel B was expected to be about 32 s, as mentioned in the section "Performance of the air-pressure-based nanofluidic control system." The fluorescence images were monitored using the fluorescence microscope and the cooled CCD camera. A sample fluorescence micrograph is shown in Fig. 5a; this was obtained for nanochannel B.

Table 1 Values of K_m, V_{max}, and k_{cat} obtained using Eqs. 2 and 3 for bulk, microfluidic, and nanofluidic reactions

	Bulk	Microfluidic	Nanofluidic
Michaelis constant [K_m(μM)]	35.1	36.5	51.2
Maximum rate [V_{max}(nMs^{-1})]	22.2	24.3	48.6
First-order rate constant [$10^{-3}k_{cat}$(s^{-1})]*	4.4	4.9	9.7

*k_{cat}=V_{max}/(total enzyme concentration)

When the scanning was performed parallel to nanochannel B, the fluorescence intensity clearly increased with distance, moving from the Y-intersection to the exit points. The distances corresponded to the reaction times in nanochannel B. Fluorescence images were acquired at various TG-β-gal concentrations, and Fig. 5b plots the reaction time and the TG-β-gal concentration dependence of the fluorescence intensity in nanochannel B. We found that the fluorescence intensity increased with increasing time and concentration across all of the experimental ranges. These results provide evidence that the enzyme reaction can even be accurately monitored in a Y-shaped extended nanospace channel. From the time courses of the fluorescence intensity, V_0 values were obtained at each TG-β-gal concentration, and the plot of $1/V_0$ vs. $1/[S]$ was compared with the results for bulk and microfluidic reactions, as shown in Fig. 4b. The trend observed for the nanofluidic reaction was different from those observed for bulk and microfluidic reactions.

Fig. 5 **a** Fluorescence micrograph of nanochannel B during the nanofluidic reaction. **b** Plot of reaction time vs. TG-β-gal concentration in nanochannel B
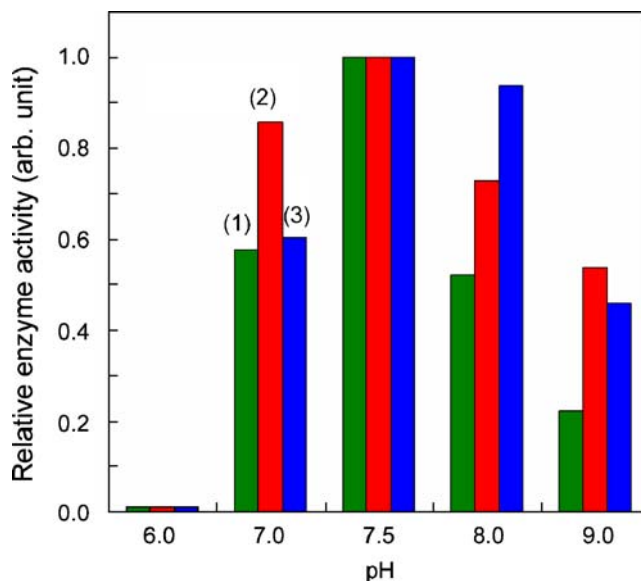
Fig. 6 pH dependence of the maximum enzyme activity for the (1) bulk, (2) microfluidic, and (3) nanofluidic reactions

The values of K_m, V_{max} and k_{cat} obtained for the nanofluidic reaction were larger than those obtained for bulk and microfluidic reactions. Their values are summarized in Table 1. These results indicate that the rate of dissociation for the enzyme in the extended nanospace does not agree with the rates observed in bulk and microspace. In particular, the k_{cat} value of 9.7×10^{-3} s^{-1} for the nanofluidics case meant that the enzyme reaction in the extended nanospace was more than twice as fast as those in bulk and microspace.

Explanations for why the enzyme reaction rate was enhanced in the extended nanospace can be broadly grouped into two types. The first was based on the adsorption of the enzyme molecules onto the surface of the extended nanospace, and the second was based on specific properties of the liquids confined in the extended nanospace. We previously investigated the effects of adsorption onto a glass substrate surface for the enzyme reaction rate, and we confirmed that the adsorbed enzyme did not have much influence on the acceleration of the rate for a short-timescale reaction (on the order of seconds) [16]. It seemed that the enhancement of the enzyme reaction rate that occurred in an extended nanospace resulted from specific properties of the confined water. The most likely candidate for such a property appears to be an enhanced proton mobility of the confined water. Previous NMR results have indicated that the proton exchange rates of the water inside the extended nanospace were enhanced due to the interactions of water with ionizable silanol groups on the glass surface, and that the proton transfer rate was enhanced by a factor of more than ten compared to the rate for bulk water [28]. If the activity of protons in water molecules induces nanospatial effects in the enzyme reaction rate, the pH dependence of the enzyme

activity for the nanofluidic-based reaction can be assumed to differ from those observed for the bulk and microfluidic reactions. Therefore, the size-confinement effects for the enzyme activity were examined at pH values of 6.0, 7.0, 7.5, 8.0, and 9.0. The maximum activities were obtained by dividing the k_{cat} values by the K_m values. A bar graph of relative enzyme activity vs. pH is shown in Fig. 6. The maximum enzyme activity was obtained for a pH of 7.5 regardless of the space size, while the pH dependence of the activity changed slightly due to the size-confinement effects. In particular, in the extended nanospace, the magnitude of the activity increased in the order of pH 7.0 <8.0<7.5. This order was different from those observed in the bulk water and water in a microspace, which increased in the order of pH 8.0<7.0<7.5. These results implied that the activity of the water protons was changed by the confinement of the water in a small space, and that our assumption that the activated protons affect the enzyme reaction rate was reasonable.

We have not been successful in establishing the size-confinement mechanisms for enhancing the enzyme reaction rate in extended nanospaces, and further studies are need to study the nanofluidic-based enzyme reaction. However, in this work, we did succeed in carrying out an important chemical reaction in an extended nanospace for the first time.

Conclusions

In the present study, we developed an air-pressure-based nanofluidic control system which included U-shaped microchannels and a Y-shaped extended nanospace channel on a glass chip, demonstrated solution mixing, and carried out an enzyme reaction in the Y-shaped extended nanospace channel. We examined the performance of the developed nanofluidic control system using the change in fluorescence intensity generated by mixing fluorescence dye and buffer solutions. The results showed that the ranges of pressure, flow rate, and residence time needed to obtain stable flow in the Y-shaped extended nanospace channel were 0.003–0.4 MPa, 0.16–21.2 pL/min, and 24 ms–32.4 s, respectively.

Furthermore, we realized the enzyme reaction in the Y-shaped extended nanospace channel by utilizing the nanofluidic control system, and evaluated the effects of size confinement on the kinetic parameters by invoking K_m, V_{max}, and k_{cat} for the enzyme reactions performed in bulk, microspace, and extended nanospace. We observed that these values increased by a factor of about two when changing from bulk and microspace to extended nanospace. The results for the pH dependence of the maximum enzyme activity suggested that the enhancement of the kinetic parameters was attributable to the enhancement of the mobility of the protons in water in the extended nanospace.

Many unclear points about the size-confinement mechanisms for the enzyme reaction still remain. However, the air-pressure-based nanofluidic control system developed here was found to have sufficient performance to measure important chemical reactions in extended nanospaces. It would be appropriate to utilize our nanofluidic control system to realize higher functional and selective chemical reactions that are impossible to achieve through bulk and microfluidic reactions. We believe that our nanofluidic apparatus and the results obtained for the enzyme reaction will have important implications for not only the evolution of micro- and nanofluidic devices, but also the understanding of chemical and biochemical reactions in extended nanospaces.

References

1. Avouris P, Chen Z, Perebeinos V (2007) Nature Nanotechnol 2:605–615
2. Ohtsu M (ed)(2006) Progress in nano-electro-optics. Springer-Verlag, Berlin
3. Goldberger J, Fan R, Yang P (2006) Acc Chem Res 39:239–248
4. Buch V, Devlin JP (eds)(2003) Water in confining geometries. Springer-Verlag, Berlin
5. Israelachvili JN (1992) Intermolecular and surface forces, 2nd edn. Academic, London
6. Bruni F, Ricci MA, Soper AK (1998a) J Chem Phys 109:1478–1485
7. Soper AK, Bruni F, Ricci MA (1998b) J Chem Phys 109:1486–1494
8. Farrer RA, Fourka JT (2003) Acc Chem Res 36:605–612
9. Pal SK, Zewail AH (2004) Chem Rev 104:2099–2123
10. Dittrich PS, Tachikawa K, Manz A (2006) Anal Chem 78:3887–3907
11. Atencia J, Beebe DJ (2005) Nature 437:648–655
12. Gunther A, Jensen KF (2006) Lab Chip 6:1487–1503
13. Song H, Ismagilov RF (2003) J Am Chem Soc 125:14613–14619
14. Mao H, Yang T, Cremer PS (2002) Anal Chem 74:379–385
15. Hadd AG, Raymond DE, Halliwell JW, Jacobson SC, Ramsey JM (1997) Anal Chem 69:3407–3412
16. Kitamori T, Tokeshi M, Hibara A, Sato K (2004) Anal Chem 76:52A–60A (and references therein)
17. Tanaka Y, Slyadnev N, Sato K, Tokeshi M, Kim H-B, Kitamori T (2001) Anal Sci 17:809–810
18. Ueno M, Hisamoto H, Kitamori T, Kobayashi S (2003) Chem Commun 936–937
19. Tamaki E, Hibara A, Kim H-B, Tokeshi M, Ooi T, Nakao M, Kitamori T (2006) Anal Sci 22:529–532
20. Goto M, Tsukahara T, Sato K, Kitamori T (2008) Anal Bioanal Chem 390:817–823
21. Eijkel JCT, van den Berg A (2005) Microfluid Nanofluid 1:249–267
22. Kaji N, Tezuka Y, Takamura Y, Ueda M, Nishimoto T, Nakanishi H, Horiike Y, Baba Y (2004) Anal Chem 76:15–22
23. Pu Q, Yun J, Temkin H, Liu S (2004) Nano Lett 4:1099–1103
24. Tegenfeldt JO, Prinz C, Cao H, Huang RL, Austin RH, Chou SY, Cox EC, Strum JC (2004) Anal Bioanal Chem 378:1678–1692
25. Guo LJ, Cheng X, Chou C-F (2004) Nano Lett 4:69–73
26. Schoch RB, Cheow LF, Han J (2007) Nano Lett 7:3895–3900
27. Hibara A, Saito T, Kim H-B, Tokeshi M, Ooi T, Nakao M, Kitamori T (2002) Anal Chem 74:6170–6176
28. Tsukahara T, Hibara A, Ikeda Y, Kitamor T (2007) Angew Chem Int Ed 46:1180–1183
29. Tamaki E, Hibara A, Kim H-B, Tokeshi M, Kitamori T (2006) J Chromatogr A 1137:256–262